Synthesis and Biologic Evaluation of a Novel ^{18}F-Labeled Adnectin as a PET Radioligand for Imaging PD-L1 Expression

David J. Donnelly*, R. Adam Smith*, Paul Morin*, Daša Lipovšek, Jochem Gokemeijer, Daniel Cohen, Virginie Lafont, Tritin Tran, Erin L. Cole, Martin Wright, Joonyoung Kim, Adrienne Pena, Daniel Kukral, Douglas D. Dischino, Patrick Chow, Jinping Gan, Olufemi Adelakun, Xi-Tao Wang, Kai Cao, David Leung, Samuel J. Bonacorsi Jr., and Wendy Hayes

Bristol-Myers Squibb Research and Development, Princeton, New Jersey

The programmed death protein (PD-1) and its ligand (PD-L1) play critical roles in a checkpoint pathway cancer cells exploit to evade the immune system. A same-day PET imaging agent for measuring PD-L1 status in primary and metastatic lesions could be important for optimizing drug therapy. Herein, we have evaluated the tumor targeting of an anti–PD-L1 adnectin after ^{18}F-fluorine labeling. **Methods:** An anti–PD-L1 adnectin was labeled with ^{18}F in 2 steps. This synthesis featured fluorination of a novel prosthetic group, followed by a copper-free click conjugation to a modified adnectin to generate ^{18}F-BMS-986192. ^{18}F-BMS-986192 was evaluated in tumors using in vitro autoradiography and PET with mice bearing bilateral PD-L1–negative (PD-L1(–)) and PD-L1–positive (PD-L1(+)) subcutaneous tumors. ^{18}F-BMS-986192 was evaluated for distribution, binding, and radiation dosimetry in a healthy cynomolgus monkey. **Results:** ^{18}F-BMS-986192 bound to human and cynomolgus PD-L1 with a dissociation constant of less than 35 pM, as measured by surface plasmon resonance. This adnectin was labeled with ^{18}F to yield a PET radioligand for assessing PD-L1 expression in vivo. ^{18}F-BMS-986192 bound to tumor tissues as a function of PD-L1 expression determined by immunohistochemistry. Radioligand binding was blocked in a dose-dependent manner. In vivo PET imaging clearly visualized PD-L1 expression in mice implanted with PD-L1(+), L2987 xenograft tumors. Two hours after dosing, a 3.5-fold-higher uptake (2.41 ± 0.29 vs. 0.82 ± 0.11 percentage injected dose per gram, $P < 0.0001$) was observed in L2987 than in control HT-29 (PD-L1(–)) tumors. Coadministration of 3 mg/kg ADX_5322_A02 anti–PD-L1 adnectin reduced tumor uptake at 2 h after injection by approximately 70%, whereas HT-29 uptake remained unchanged, demonstrating PD-L1–specific binding. Biodistribution in a nonhuman primate showed binding in the PD-L1–rich spleen, with rapid blood clearance through the kidneys and bladder. Binding in the PD-L1(+) spleen was reduced by coadministration of BMS-986192. Dosimetry estimates indicate that the kidney is the dose-limiting organ, with an estimated human absorbed dose of 2.20E–01 mSv/MBq. **Conclusion:** ^{18}F-BMS-986192 demonstrated the feasibility of noninvasively imaging the PD-L1 status of tumors by small-animal PET studies. Clinical studies with ^{18}F-BMS-986192 are under way to measure PD-L1 expression in human tumors.

Received Jul. 31, 2017; revision accepted Sep. 19, 2017.

For correspondence or reprints contact: David J. Donnelly, Bristol-Myers Squibb Pharmaceutical Research and Development, P.O. Box 4000, Princeton, NJ 08543.

E-mail: david.donnelly@bms.com

*Contributed equally to this work.

Published online Oct. 12, 2017.

Key Words: PD-L1; PET; PD-1/PD-L1 checkpoint inhibitor; ^{18}F-labeled Adnectin; ^{18}F-BMS-986192

J Nucl Med 2018; 59:529–535
DOI: 10.2967/jnumed.117.199596

A healthy immune system maintains a delicate balance between eradicating infections/cancers and maintaining self-tolerance. The immune system accomplishes this in part by the expression of immune checkpoints that control immune response. However, tumors exploit these checkpoint pathways by expressing coinhibitory proteins to evade antitumor immune responses (*1*). One major checkpoint inhibitor pathway is the PD-1 pathway. PD-1 is a negative costimulatory receptor expressed on the surface of activated T and B cells (*2,3*). PD-L1 is a surface glycoprotein ligand for PD-1 that facilitates immunosuppression on both antigen-presenting cells and human cancers. PD-L1 downregulates T-cell activation and cytokine secretion by binding to PD-1 (*4,5*). Several antibodies directed against the PD-1/PD-L1 pathway have been developed to treat a wide variety of cancers (*6–10*). Elevated PD-L1 expression is correlated with poor prognosis in some cancers, which suggests that PD-L1 upregulation is a mechanism for tumor immune evasion (*11*). The predictive role of PD-L1 expression on tumor cells has been an active area of research, and several immunohistochemistry assays have been developed to predict responses to either anti–PD-1 or anti–PD-L1 treatment (*12*). However, these measures are limited as typically only a single patient biopsy sample is evaluated for PD-L1 expression using immunohistochemistry (*13,14*). A PD-L1 PET radioligand represents a noninvasive tool that is complementary to immunohistochemistry, which allows for serial imaging of PD-L1 expression in both primary and metastatic tumors. In addition, this tool could measure in vivo dynamic changes in PD-L1 expression during and after treatment with immune checkpoint–modulating drugs without needle biopsy (*15*).

Recently, there has been a resurgence in the application of antibody-based imaging agents, and several imaging agents targeting PD-L1 have recently been reported in the literature using this framework (*16–21*). These agents offer the affinity and specificity needed to maximize signal-to-background ratios for visualizing a molecular target within the tumor microenvironment. However, one disadvantage of antibody-based imaging agents is their slow clearance. Typically, antibodies are cleared through the hepatobiliary system over a period of days to weeks, making

imaging in neighboring organs such as the lung a challenge. As a result, it can take many days for these agents to sufficiently clear target-free tissues or neighboring tissues to enable imaging. An ideal PD-L1 PET radioligand is one that offers high tumor uptake in PD-L1–positive (PD-L1(+)) tumors and low background signal in non-PD-L1–expressing tissues and enables same-day imaging for patients for flexibility in clinical study design (*22*).

Adnectins are a family of engineered, target-binding proteins that are derived from the 10th type III domain of human fibronectin (10Fn3). The 10Fn3 structure resembles antibody-variable domains, having 2 sets of antiparallel β-sheets with solvent-accessible loops at each pole (*23,24*). These loops can be engineered to provide high binding affinity to a wide variety of targets. Adnectins have several advantages as targeting domains for molecular imaging agents. Their smaller size (~10 kDa) allows for good image contrast with rapid delivery to targeted tissues and fast glomerular clearance of unbound probe to drive image contrast. Adnectins have high stability, and the absence of cysteine or disulfide bonds allows the introduction of a single cysteine for site-specific conjugation of PET radionuclides. Herein is presented the preliminary evaluation of a ^{18}F-labeled adnectin as a same-day in vivo PET radioligand to quantify PD-L1 expression in tumors.

MATERIALS AND METHODS

Adnectin production and conjugation of DBCO with ADX_5322_A02, surface plasmon resonance, immunohistochemistry, fluorescence-activated cell sorting, cell lines, and radiation dosimetry are found in the supplemental materials (available at http://jnm.snmjournals.org).

Synthesis of ^{18}F-BMS-986192

^{18}F-fluoride (29.6 GBq) was transferred through a preconditioned anion exchange cartridge and eluted with potassium carbonate (3 mg) and 4,7,13,16,21,24-hexaoxa-1,10-diazabicyclo[8.8.8]hexacosane (15 mg) in 1.4 mL of acetonitrile. The solvent was azeotroprically dried, and to this mixture was added 3-(2-(2-(2-(2-azidoethoxy)ethoxy)ethoxy)ethoxy)-2-nitropyridine (2 mg) in 0.5 mL of dimethyl sulfoxide. This solution was heated at 120°C for 10 min, followed by dilution with 3 mL of water and transferred onto a Luna C18 (250 × 10 mm) high-performance liquid chromatography column. The prosthetic group ^{18}F-BMT-187144 was purified using a mobile phase mixture of 32% acetonitrile in 0.1% trifluoroacetic acid at a flow rate of 4.6 mL/min. ^{18}F-BMT-187144 was collected into a 100-mL flask that contained 25 mL of water, and its contents were delivered to a C18 cartridge. ^{18}F-BMT-187144 was released from the cartridge with 3 mL of ethanol, evaporated to dryness, and reconstituted into 0.1 mL of sterile water. To this solution was added 0.2 mL of ADX_5322_A02-DBCO (3 mg/mL) in phosphate-buffered saline (PBS). The reaction mixture was gently mixed for 45 min at 45°C. ^{18}F-BMS-986192 was purified using a Superdex 200 10/300 GL size-exclusion column and 1× PBS mobile phase at a 0.5 mL/min flow rate. ^{18}F-BMS-986192 was isolated over a 5-min period and passed through a 0.2-μm polyethersulfone membrane filter and into a sterile vial as the final formulated product. The radiochemical purity was determined using a high-performance liquid chromatography (Agilent) system and a Posi-Ram (INUS) radio–high-performance liquid chromatography detector. Methods for quality control and specific activity of ^{18}F-BMS-986192 are found in the supplemental materials (Supplemental Figs. 1–3).

Animal Models

All procedures involving animal studies were reviewed and approved by the Bristol-Myers Squibb animal care and use committee. In vivo studies were performed by implanting tumor xenografts in 5- to 6-wk-old female athymic nude mice (Charles River). The L2987 is a human lung carcinoma cell line, and the HT-29 is a colon adenocarcinoma carcinoma cell line (American Type Culture Collection). Bilateral tumor xenografts were established by subcutaneous inoculation of HT-29 (1.5E06 cells) and L2987 (4E06 cells) in contralateral shoulders in a total injection volume of 0.2 mL. Once tumors reached approximately 300 mm^3, animals were selected for imaging.

Autoradiography

HT-29/L2987 tumors were excised 2 wk from the implantation date. Replicate sets of 5-μm-thick cryosections were prepared and adhered to glass slides. Fresh frozen human non–small cell lung cancer (NSCLC) tumor samples (5 μm) were also obtained (Asterand). Slides were preincubated for 20 min using a protein block solution (Dako), then transferred to glass incubation chambers that contained 40 mL of buffer (1× PBS supplemented with 0.5% bovine serum albumin) and a 0.25 nM solution of ^{18}F-BMS-986192. Several samples were coincubated with BMS-986192 at 0.025, 0.25, 2.5, and 25 nM or a non-PD-L1–binding (sham) adnectin (25 nM). These slides were incubated for 1 h at room temperature and then were washed 4 times with ice-cold buffer for 3 min. Slides were air dried at room temperature and affixed to a phosphorimaging plate (BAS-SR 3545S) and exposed for 15 min. Plates were scanned using a bioimaging analyzer (FLA-9000; Fujifilm). Images were analyzed using multigauge software.

Small-Animal PET Imaging

Mice were anesthetized with isoflurane in oxygen (2% induction and maintenance); tail vein catheters were installed then transferred to the microPET F120 scanner (Siemens). A 10-min transmission image was acquired using a ^{57}Co point source for attenuation correction of the final PET images. Then approximately 5.6 MBq of ^{18}F-BMS-986192 (n = 7) were administered via the tail vein. Two-hour dynamic emission images were acquired for all animals. For blocking studies, animals (n = 4) received 3 mg/kg ADX_5322_A02 anti–PD-L1 adnectin coadministered with ^{18}F-BMS-986192. PET data were reconstructed using a 3-dimensional ordered-subsets expectation maximization followed by maximum a posteriori algorithm corrected for attenuation using the previously acquired transmission scan. Images were analyzed using ASIPro software (Siemens), with regions of interest drawn around tumors and radiotracer uptake expressed as percentage injected dose per gram (%ID/g).

Ex Vivo Biodistribution

^{18}F-BMS-986192 was also coadministered for ex vivo biodistribution studies with varying concentrations of BMS-986192 in a single syringe to alter the effective specific activity of the administered tracer dose. Animals in each group (n = 4) received approximately 5.6 MBq of ^{18}F-BMS-986192 with effective specific activities of 14.1, 7.1, 2.8, 1.4, or 0.7 MBq/nmol. Ninety minutes after injection, the mice were euthanized and the blood, liver, kidneys, spleen, heart, lung, stomach, muscle, bone, HT-29, and L2987 tumors were collected and measured using a γ-counter (Wallac3; Perkin-Elmer).

Cynomolgus PET Imaging

Animals were anesthetized with an intramuscular injection of 0.02 mg/kg atropine, 5 mg/kg Telazol (tiletamine HCl and zolazepam HCl), and 0.01 mg/kg buprenorphine. Catheters were placed into the saphenous and cephalic veins, and animals were intubated and transferred to the microPET F220 (Siemens). Anesthesia was maintained with isoflurane and oxygen. Intravenous fluids (lactated ringers solution) were administered throughout the scan. Transmission images using a

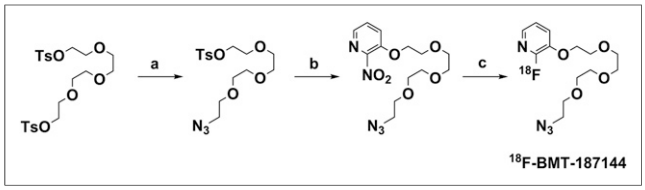

FIGURE 1. Synthesis of ^{18}F-BMT-187144. Reagents and conditions: a) NaN_3, ethanol 90°C 17 h; b) NaH, 2-nitropyridin-3-ol 0–60°C, 4 h; c) K.2.2.2 K^{18}F, dimethyl sulfoxide 120°C 10 min.

^{57}Co point source were acquired over 5 individual bed positions (10 min per position) to image from the top of head to lower leg of the animal. Adjacent bed positions were set to overlap by 1.5 cm. ^{18}F-BMS-986192 (~55.5 MBq) was administered via the saphenous catheter. Emission images were acquired in a sequence of 5 passes over the previous 5 bed positions (5 min per position), producing a series of whole-body images covering a duration of about 150 min after tracer administration. Images were reconstructed using a filtered backprojection algorithm with attenuation correction using the ^{57}Co transmission scans and corrected for decay. A blocking study in the same nonhuman primate was conducted 24 h after the first baseline imaging study. This study followed the procedure described above, only tracer was coadministered with 1 mg/kg BMS-986192.

RESULTS

Selection and Radiolabeling of Anti–PD-L1 Adnectin

An anti–PD-L1 adnectin (ADX_5322_A02) was selected in vitro, produced, characterized, and successfully labeled with ^{18}F. Surface plasmon resonance analysis was used to determine the kinetic parameters of ADX_5322_A02 and BMS-986192 as it bound to human or cynomolgus PD-L1 (Supplemental Fig. 4). BMS-986192 shows no appreciable difference in binding parameters to its unmodified counterpart ADX_5322_A02 (Supplemental Table 1). This adnectin displayed picomolar dissociation constants (<35 pM) against both human and cynomolgus PD-L1 (near the limit of detection via surface plasmon resonance) and did not bind to murine PD-L1 (Supplemental Table 2).

A ^{18}F-labeled derivative of ADX_5322_A02 anti–PD-L1 adnectin was synthesized using a ^{18}F prosthetic group, ^{18}F-BMT-187144 (Fig. 1). ^{18}F-BMT-187144 was generated in high radiochemical yield (>70% non–decay-corrected yield, $n = 40$), in greater than 90% radiochemical purity, was stable in a PBS solution over 1 h, and was reduced to dryness without loss of radioactivity, enabling efficient protein labeling with ^{18}F (supplemental materials). The ^{18}F-BMT-187144 prosthetic group was then used to synthesize ^{18}F-BMS-986192 as shown in Figure 2, using copper-free click chemistry. ^{18}F-BMS-986192 (1.1 ± 0.3 GBq [$n = 15$]) was isolated, starting from 29.6 GBq of ^{18}F-fluoride with 96% ± 3% radiochemical purity and a specific activity of 63 ± 3 MBq/nmol.

Characterization of PD-L1 Expression in HT-29 and L2987 Xenografts

HT-29 and L2987 xenograft tumor models were investigated regarding PD-L1 expression using fluorescence-activated cell sorting, immunohistochemistry, autoradiography, and in vivo biodistribution in an immunocompromised mouse model. Fluorescence-activated cell sorting of these cells and immunohistochemistry analysis of xenograft tissues derived from these cell lines showed moderate expression of PD-L1 in the L2987 model whereas HT-29 was confirmed as a negative control with little or no PD-L1 expression (Figs. 3A and 3B). Autoradiography of these xenograft tissues showed increased ^{18}F-BMS-986192 binding to L2987 (14.0 ± 1.0 PSL/mm^2) compared with control HT-29 (1.59 ± 0.5 PSL/mm^2) (Fig. 3C).

Autoradiography in Human NSCLC Tissue Samples

^{18}F-BMS-986192 binding was assessed in a panel of 6 human NSCLC samples (Fig. 3C). ^{18}F-BMS-986192 exhibited increased total radioligand binding in all the tested human tissues compared with the xenograft tissues, ranging from 21.35 to 230.79 PSL/mm^2 (Table 1). Specificity of binding to tissue samples was evaluated in blocking studies by coincubation with excess BMS-986192. Dose-dependent blockade of ^{18}F-BMS-986192 binding to all PD-L1–positive tissues was seen with increasing concentration of blocking agent (Fig. 3C; Table 1). At a 25 nM concentration of BMS-986192, radiotracer binding was reduced by 75%–95% in the human NSCLC tissue samples. Coincubation with 25 nM of a non-PD-L1–binding sham adnectin resulted in no appreciable change in radiotracer binding to any tissue sample, confirming the specificity of ^{18}F-BMS-986192 binding. ^{18}F-BMS-986192 binding demonstrated concordance with PD-L1 immunohistochemistry staining (Figs. 3B and 3C) in human NSCLC tissues.

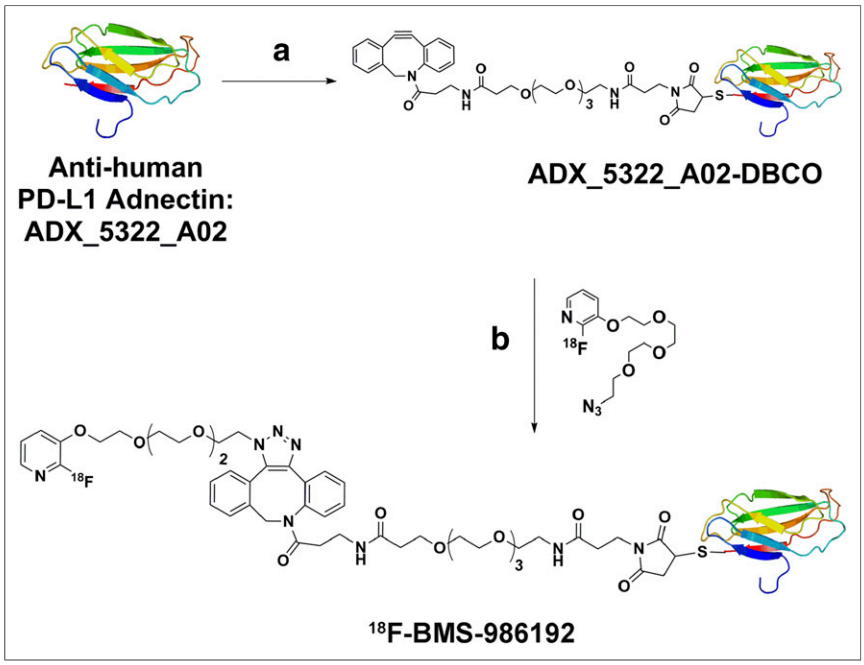

FIGURE 2. Synthesis of ^{18}F-BMS-986192. Reagents and conditions: a) Maleimide-PEG4-DBCO 25°C, 1 h 1× PBS, pH 7.4/dimethyl sulfoxide; b) 1× PBS for 45 min.

Small-Animal PET Imaging and Biodistribution

To evaluate the potential of ^{18}F-BMS-986192 as a PET radioligand for PD-L1, PET imaging in xenograft models was

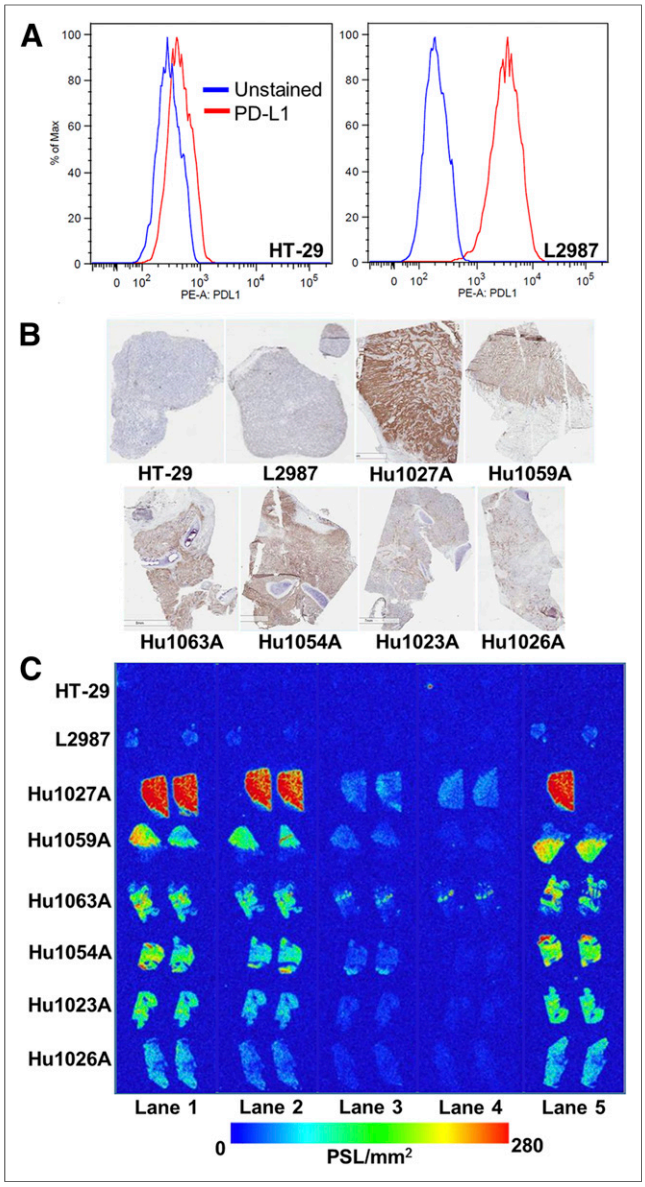

FIGURE 3. (A) Fluorescence-activated cell sorting analysis of HT-29 and L2987 cells. (B) Anti–PD-L1 immunohistochemistry staining of xenograft and human NSCLC tissues. (C) In vitro autoradiography of xenograft and human NSCLC tissue samples using ^{18}F-BMS-986192. Lane (1): total binding of ^{18}F-BMS-986192, lane (2) 0.25 nM BMS-986192 blocking, lane (3) 2.5 nM BMS-986192 blocking, lane (4) 25 nM BMS-986192 blocking, and lane (5) 25 nM non-PD-L1–binding sham adnectin control.

performed. Representative PET whole-body coronal images of mice with bilateral HT-29 and L2987 xenografts demonstrated increased accumulation of ^{18}F-BMS-986192 in the moderate PD-L1–expressing L2987 compared with control HT-29 tumors with negligible PD-L1 expression (2.41 ± 0.29 vs. 0.82 ± 0.11 %ID/g, $P < 0.0001$; Fig. 4A). Tracer uptake in peripheral organs (e.g., liver, lung, and heart) was moderate, and uptake in muscle was minimal, resulting in high-contrast images. Tracer accumulation in L2987 tumors plateaued between 90 and 120 min after tracer administration (Fig. 4B).

Specificity of ^{18}F-BMS-986192 binding was further confirmed in blocking studies in which excess BMS-986192 was coinjected along with the radiotracer. Accumulation of ^{18}F-BMS-986192 in L2987 tumors was reduced by 70% compared with mice that received the radiotracer alone (Fig. 4A). Resulting uptake in PD-L1(+) L2987 tumors was similar to that in the PD-L1–negative (PD-L1(−)) HT-29 tumor (0.79 ± 0.12 vs. 0.71 ± 0.15 %ID/g, $P = 0.44$), demonstrating near-complete blockade of specific tracer uptake and suggesting that tumor accumulation of ^{18}F-BMS-986192 in the L2987 xenograft model was consistent with specific binding. Ex vivo biodistribution studies confirmed significantly higher uptake in L2987 compared with control HT-29 tumors and with other peripheral tissues (Fig. 5A). Tracer uptake was 3.5- to 4-fold higher than in PD-L1(−) HT-29 control tumors. The only tissue with higher uptake was the kidney, which is consistent with its role in clearance. The ratio of tracer uptake in L2987 tumors to various background tissues (HT-29 tumor, muscle, and blood) was measured after coadministration of increasing doses of BMS-986192 (Fig. 5B). These studies indicated a dose-dependent blockade of radiotracer accumulation in L2987 tumors, resulting in a reduced uptake ratio. The highest blocking dose (tracer specific activity of 0.7 MBq/nmol) showed a complete elimination of tumor contrast, confirming the specific nature of ^{18}F-BMS-986192 binding in vivo.

Cynomolgus Imaging

PET imaging in a healthy cynomolgus monkey using ^{18}F-BMS-986192 showed an accumulation of tracer in the PD-L1(+) spleen tissue, reaching a 12-to-1 ratio compared with muscle. Overall background signal was low, with little accumulation outside the spleen and clearance organs of kidney and urinary bladder (Fig. 6A). Accumulation in the PD-L1(+) spleen was reduced approximately 90% to near-background levels with coadministration of 1 mg/kg BMS-986192 (Fig. 6B), reducing the spleen-to-muscle ratio to 1.24:1. The reduction of specific radiotracer accumulation in the spleen is consistent with moderate PD-L1 staining seen by immunohistochemistry (Fig. 6C).

Dosimetry results indicate that the distribution of ^{18}F-BMS-986192 is similar between male and female animals. The kidney is the dose-limiting organ with an estimated absorbed dose for the average human subject of 2.20E−01 mSv/MBq (Supplemental Table 3). Under Radioactive Drug Research Committee exposure limits as specified in 21 CFR 361.1, this yields an estimated single study administration dose of 228 MBq for the average human subject.

DISCUSSION

The goal of this work was to develop an ^{18}F-labeled radioligand to enable noninvasive, same-day imaging of PD-L1 expression in living tissues. This tool allows for a longitudinal measurement of PD-L1 expression within the tumor microenvironment before, during, and after therapeutic intervention. Recently, several PD-L1 imaging agents have demonstrated feasibility of evaluating PD-L1 expression (*16,19,20,25,26*).

Adnectins are an attractive scaffold for same-day PET imaging of this target as they demonstrate high target affinity and rapid tumor uptake. Similar to peptide-based scaffolds, adnectins also have rapid clearance from blood and background tissues (*26–29*). A recent study with an epidermal growth factor receptor (EGFR)–binding adnectin labeled with a PET radionuclide showed the feasibility of using this scaffold to generate a tracer targeting EGFRs in tumors with high signal-to-noise ratios (*28*).

^{18}F is an attractive radionuclide for labeling adnectins given its 97% emission via positron emission, high theoretic specific

TABLE 1
^{18}F-BMS-986192 In Vitro Autoradiography

Tissue	Total binding	+ BMS-986192 blocking				+ Sham, 25 nM
		0.025 nM	0.25 nM	2.5 nM	25 nM	
HT29	3.59	3.67	3.94	4.02	4.14	3.40
L2987	9.58	7.16	6.04	4.21	4.92	8.92
Hu1027A*	230.79	210.01	191.72	12.03	12.63	182.07
Hu1059A*	89.43	72.17	50.83	10.09	5.23	86.46
Hu1063A*	40.99	41.75	26.18	10.12	10.36	33.24
Hu1054A*	55.96	49.89	32.39	9.28	4.20	67.11
Hu1023A*	42.78	30.80	21.89	6.76	4.52	40.72
Hu1026A*	21.35	17.96	11.32	5.46	4.85	24.59

*Denotes human NSCLC tumor sample.
All values reported as mean PSL/mm^2.

activity of 63 TBq/μmol, and 109.5 min half-life, which matches the less than 2-h blood half-life of adnectins in humans (*23,30*). To incorporate ^{18}F labeling, the adnectin was engineered with a cysteine residue on the c terminus of the protein, on the opposite pole of the variable loops assumed to confer PD-L1 binding. This placement allowed the PET labeling motifs to be attached distal from the PD-L1 recognition residues. Surface plasmon resonance data confirmed that these modifications did not have an effect on the binding of this adnectin, which remained in the picomolar range. The strategy for ^{18}F labeling was to conjugate the anti–PD-L1 adnectin with a ^{18}F prosthetic group using copper-free click chemistry and a commercially available ring-constrained DBCO-PEG4-maleimide moiety. This bioorthogonal agent enabled site-specific modification at the engineered cysteine residue without compromising the stability or affinity of the adnectin protein.

Efforts were made to use previously described prosthetic groups to label the adnectin platform with ^{18}F, including the azide containing 1-azido-2-(2-(2-(2-fluoroethoxy)ethoxy)ethoxy)ethane (*31*). Unfortunately, this approach did not yield the desired product. Under dilute reaction conditions needed to keep the total volume of ethanol in the reaction solution below 10% (for adnectin stability) no ^{18}F labeling occurred. Attempts to concentrate the crude reaction solution led to ethanol concentrations above 10%, which led to aggregation of the adnectin. Further attempts to concentrate this prosthetic group in solution volatilized the product. To solve this issue, a nitropyridine was incorporated (Fig. 1), which allowed for rapid ^{18}F incorporation into the molecule and provided a nonvolatile prosthetic group. This allowed for the complete removal of organic solvents with minimal radioactivity loss (Supplemental Table 4). The product could then be reconstituted in aqueous buffer for stability of the adnectin. The novel labeled prosthetic group was stable in this buffer system for over an hour (Supplemental Fig. 5) and enabled efficient ^{18}F labeling of the PD-L1 adnectins.

^{18}F-BMS-986192 shows PD-L1–specific uptake in tumor tissues. In vitro autoradiography experiments demonstrated higher binding to PD-L1(+) than to PD-L1(−) xenograft tissues in a 9:1 ratio. Studies with human NSCLC tissues demonstrated similar results (Fig. 3C). ^{18}F-BMS-986192 binding in human NSCLC tissues was proportional to PD-L1 staining by immunohistochemistry (Figs. 3B and 3C). Coadministration with BMS-986192 reduced radioligand binding in both the human NSCLC and the L2987 xenograft tissues by more than 80%, with minimal effect observed in PD-L1(−) tissues. Finally, radioligand binding of ^{18}F-BMS-986192 was not affected by coadministration of a non–PD-L1 binding sham adnectin (Fig. 3C). These results suggest ^{18}F-BMS-986192 retains its high affinity and specificity to the PD-L1 receptor.

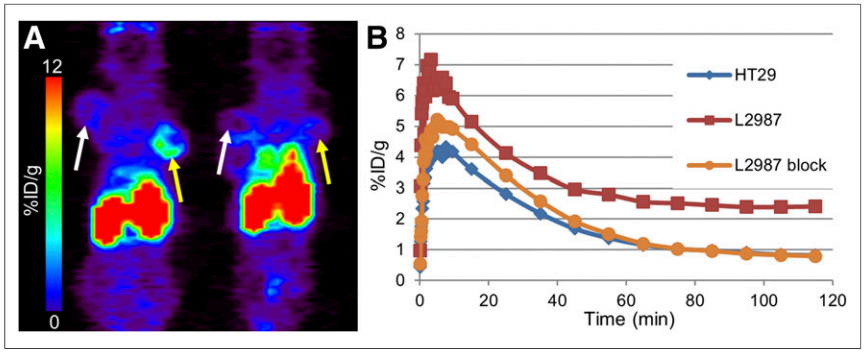

FIGURE 4. (A) Representative coronal PET images (slices) of 2 mice bearing bilateral PD-L1(+) L2987 (yellow arrows) and PD-L1(−) HT-29 (white arrows) tumors at 90–120 min after ^{18}F-BMS-986192 administration. Left image shows tracer alone; right image shows coadministration of 3 mg/kg BMS-986192. (B) Representative time–activity curves.

PET imaging with this tracer in mice implanted with both PD-L1(+) and PD-L1(−) xenografts demonstrated rapid accumulation in the PD-L1(+) tumor and minimal signal in the PD-L1(−) tumor (Fig. 4). Using ^{18}F-BMS-986192, we visualized the PD-L1(+) xenograft in a 3.6:1 ratio over the PD-L1(−) tumor in vivo and the tumor-to-muscle ratio remained high (>11:1), providing high-contrast images (Fig. 4A). Coinjection of BMS-986192 reduced accumulation of the radioligand in PD-L1(+) tumors by more than 70% to a

level similar to the PD-L1(−) tumor, confirming the specific nature of ^{18}F-BMS-986192 accumulation in L2987 xenografts (Figs. 4B and 4C). Collectively, the in vitro and in vivo results show that ^{18}F-BMS-986192 can be used to measure PD-L1 expression in tumors.

Because ^{18}F-BMS-986192 does not bind to mouse PD-L1, a study was performed to understand biodistribution in a model with endogenous PD-L1 expression. Picomolar dissociation constants were observed in a nonhuman primate and immunohistochemistry showed moderate PD-L1 expression in the cynomolgus spleen (Fig. 6C). PET studies confirmed that background accumulation of ^{18}F-BMS-986192 was minimal, with little signal outside the spleen, kidney, and urinary bladder (Fig. 6A). Accumulation in the PD-L1(+) spleen of the same nonhuman primate was reduced to background with coadministration of 1 mg/kg BMS-986192 (Fig. 6B). The reduction of radiotracer accumulation in the spleen is consistent with specific binding, because moderate PD-L1 staining was seen by immunohistochemistry (Fig. 6C).

The advantages of the ^{18}F-adnectin platform described herein have been demonstrated through experiments with ^{18}F-BMS-986192. Time–activity curves showed ^{18}F-BMS-986192 rapidly cleared through the kidney, with peak radioactivity observed at 25 min after injection in mice. Given the prolonged kidney retention observed with similar protein-based tracers using chelating agents or prolonged liver clearance seen with monoclonal antibody tracers coupled with the clinical utility of same-day imaging, the advantages of ^{18}F-BMS-986192 as a PD-L1 radioligand are clear (*32*). No radioactive metabolites were seen with ^{18}F-BMS-986192 2 h after injection, and pharmacokinetic studies show BMS-986192 is excreted as an intact molecule (Supplemental Figs. 6 and 7). From an imaging perspective, renal clearance of ^{18}F-BMS-986192 offers a distinct advantage over monoclonal antibody imaging agents for PD-L1 that are cleared through the liver depositing their radiometal when catabolized, potentially masking tumors therein. The rapid blood clearance of ^{18}F-BMS-986192 provides an advantage compared with other monoclonal antibody–based PD-L1 immuno-PET agents such as ^{64}Cu/^{89}Zr-atezolizumab that require imaging several days after injection of the tracer (*20*).

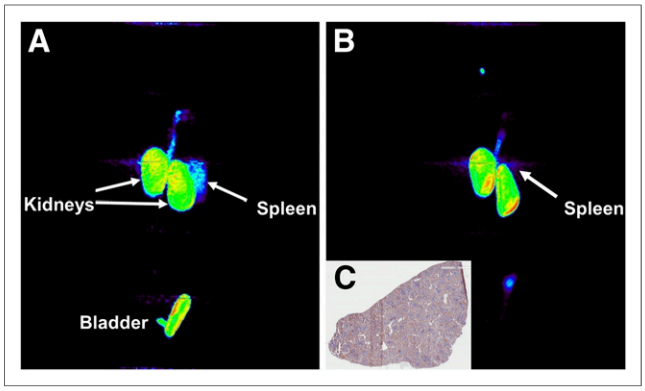

FIGURE 6. Representative whole-body PET (maximal-intensity projection) images 90 min after injection of (A) ^{18}F-BMS-986192 only and (B) ^{18}F-BMS-986192 with a coadministration of 1 mg/kg BMS-986192 in the same monkey. (C) Representative anti–PD-L1 immunohistochemistry of healthy monkey spleen tissue.

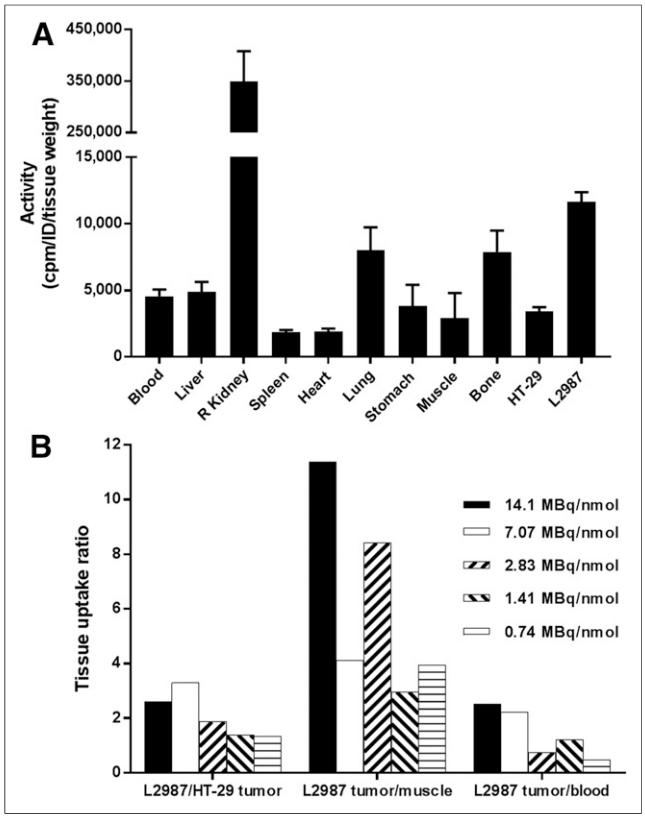

FIGURE 5. (A) Ex vivo biodistribution of ^{18}F-BMS-986192 in mice implanted with L2987 and HT-29 xenografts. Bars indicate mean ± SD (n = 4). (B) Contrast ratio of L2987 tumor uptake compared with control HT-29 tumors, skeletal muscle, and blood.

CONCLUSION

A novel ^{18}F-labeled adnectin radioligand was developed for PET imaging of PD-L1–expressing tissues. In addition, an improved methodology was described based on a unique prosthetic group that allows for the ^{18}F labeling of adnectins under mild conditions. Using copper-free click chemistry, we generated ^{18}F-BMS-986192 with picomolar affinity toward the human PD-L1 receptor in high radiochemical purity and high specific activity. This methodology addresses important issues associated with the ^{18}F labeling of proteins and should be applicable to related systems. In vivo imaging demonstrated rapid delivery of ^{18}F-BMS-986192 to PD-L1–expressing tumors and rapid clearance from non-PD-L1–expressing tumors and tissues. ^{18}F-BMS-986192 was highly stable in vivo and had low background signals in organs of interest such as the lung. The results of this study demonstrate the feasibility of preparing ^{18}F anti–PD-L1 adnectins for the measurement of PD-L1 expression in tumors. Radiation dosimetry estimates indicate that this tracer is safe to administer in human studies. Clinical studies with ^{18}F-BMS-986192 are currently under way to better understand this checkpoint pathway and PD-L1 expression in human tumors.

DISCLOSURE

All authors are employed by Bristol-Myers Squibb Co. ^{18}F-BMS-986192 and ^{18}F-BMT-187144 are the subject of patent applications WO2016086021A1 and WO2016086036A2. No other potential conflict of interest relevant to this article was reported.

ACKNOWLEDGMENTS

We thank Amy Bertino, Alex Bush, Elliot Ethridge, David Fabrizio, Pallavi Gambhire, Ben Henley, Zheng Lin, David Linsenmayer, Sarah Maas, Frank Marsilio, Doug McLaughlin, Tracy Mitchell, John Newitt, Ted Pellas, Michael Pietras, Katie Russo, and Kevin Smith for their efforts in support of the work generated in this manuscript.

REFERENCES

1. Pardoll DM. The blockade of immune checkpoints in cancer immunotherapy. *Nat Rev Cancer.* 2012;12:252–264.
2. Riella LV, Paterson AM, Sharpe AH, Chandraker A. Role of the PD-1 pathway in the immune response. *Am J Transplant.* 2012;12:2575–2587.
3. Keir ME, Butte MJ, Freeman GJ, Sharpe AH. PD-1 and its ligands in tolerance and immunity. *Annu Rev Immunol.* 2008;26:677–704.
4. Herbst RS, Soria JC, Kowanetz M, et al. Predictive correlates of response to the anti-PD-L1 antibody MPDL3280A in cancer patients. *Nature.* 2014;515:563–567.
5. Freeman GJ, Long AJ, Iwai Y, et al. Engagement of the PD-1 immunoinhibitory receptor by a novel B7 family member leads to negative regulation of lymphocyte activation. *J Exp Med.* 2000;192:1027–1034.
6. Kazandjian D, Suzman DL, Blumenthal G, et al. FDA approval summary: Nivolumab for the treatment of metastatic non-small cell lung cancer with progression on or after platinum-based chemotherapy. *Oncologist.* 2016;21:634–642.
7. Gyawali B, Ota A, Ando Y. Nivolumab in nonsquamous non-small-cell lung cancer. *N Engl J Med.* 2016;374:493.
8. Borghaei H, Brahmer J. Nivolumab in nonsquamous non-small-cell lung cancer. *N Engl J Med.* 2016;374:493–494.
9. Herbst RS, Baas P, Kim DW, et al. Pembrolizumab versus docetaxel for previously treated, PD-L1-positive, advanced non-small-cell lung cancer (KEYNOTE-010): a randomised controlled trial. *Lancet.* 2016;387:1540–1550.
10. Weinstock M, McDermott D. Targeting PD-1/PD-L1 in the treatment of metastatic renal cell carcinoma. *Ther Adv Urol.* 2015;7:365–377.
11. He J, Hu Y, Hu M, Li B. Development of PD-1/PD-L1 pathway in tumor immune microenvironment and treatment for non-small cell lung cancer. *Sci Rep.* 2015; 5:13110.
12. Chakravarti N, Prieto VG. Predictive factors of activity of anti-programmed death-1/programmed death ligand-1 drugs: immunohistochemistry analysis. *Transl Lung Cancer Res.* 2015;4:743–751.
13. Topalian SL, Taube JM, Anders RA, Pardoll DM. Mechanism-driven biomarkers to guide immune checkpoint blockade in cancer therapy. *Nat Rev Cancer.* 2016;16:275–287.
14. Patel SP, Kurzrock R. PD-L1 Expression as a predictive biomarker in cancer immunotherapy. *Mol Cancer Ther.* 2015;14:847–856.
15. Ilie M, Long-Mira E, Lassalle S, et al. Comparative study of the PD-L1 status between surgically resected specimens and matched biopsies of NSCLC patients reveal major discordances: a potential issue for anti-PD-L1 therapeutic strategies. *Ann Oncol.* 2016;27:147–153.
16. Chatterjee S, Lesniak WG, Gabrielson M, et al. A humanized antibody for imaging immune checkpoint ligand PD-L1 expression in tumors. *Oncotarget.* 2016;7:10215–10227.
17. Wu AM. Antibodies and antimatter: the resurgence of immuno-PET. *J Nucl Med.* 2009;50:2–5.
18. Wu AM. Engineering multivalent antibody fragments for *in vivo* targeting. In: Lo BKC, ed. *Antibody Engineering: Methods and Protocols.* Totowa, NJ: Humana Press; 2004:209–225.
19. Hettich M, Braun F, Bartholoma MD, Schirmbeck R, Niedermann G. High-resolution PET imaging with therapeutic antibody-based PD-1/PD-L1 checkpoint tracers. *Theranostics.* 2016;6:1629–1640.
20. Lesniak WG, Chatterjee S, Gabrielson M, et al. PD-L1 detection in tumors using ^{64}Cu-atezolizumab with PET. *Bioconjug Chem.* 2016;27:2103–2110.
21. Heskamp S, Hobo W, Molkenboer-Kuenen JD, et al. Noninvasive imaging of tumor PD-L1 expression using radiolabeled anti-PD-L1 antibodies. *Cancer Res.* 2015;75:2928–2936.
22. Olafsen T, Sirk SJ, Olma S, Shen CKF, Wu AM. ImmunoPET using engineered antibody fragments: fluorine-18 labeled diabodies for same-day imaging. *Tumour Biol.* 2012;33:669–677.
23. Lipovšek D. Adnectins: engineered target-binding protein therapeutics. *Protein Eng Des Sel.* 2011;24:3–9.
24. Koide A, Koide S. Monobodies: antibody mimics based on the scaffold of the fibronectin type III domain. *Methods Mol Biol.* 2007;352:95–109.
25. Maute RL, Gordon SR, Mayer AT, et al. Engineering high-affinity PD-1 variants for optimized immunotherapy and immuno-PET imaging. *Proc Natl Acad Sci USA.* 2015;112:E6506–E6514.
26. Chatterjee S, Lesniak WG, Miller MS, et al. Rapid PD-L1 detection in tumors with PET using a highly specific peptide. *Biochem Biophys Res Commun.* 2017; 483:258–263.
27. Rossin R, Berndorff D, Friebe M, Dinkelborg LM, Welch MJ. Small-animal PET of tumor angiogenesis using a ^{76}Br-labeled human recombinant antibody fragment to the ED-B domain of fibronectin. *J Nucl Med.* 2007;48: 1172–1179.
28. Hackel BJ, Kimura RH, Gambhir SS. Use of ^{64}Cu-labeled fibronectin domain with EGFR-overexpressing tumor xenograft: molecular imaging. *Radiology.* 2012; 263:179–188.
29. Natarajan A, Hackel BJ, Gambhir SS. A novel engineered anti-CD20 tracer enables early time PET imaging in a humanized transgenic mouse model of B-cell non-Hodgkins lymphoma. *Clin Cancer Res.* 2013;19:6820–6829.
30. Weissleder R, Ross BD, Rehemtulla A, Gambhir SS. *Molecular Imaging, Principles and Practices*. Vol. 13. Shelton, CT: Peoples Medical Publishing House–USA; 2011.
31. Gill HS, Marik J. Preparation of ^{18}F-labeled peptides using the copper(I)-catalyzed azide-alkyne 1,3-dipolar cycloaddition. *Nat Protoc.* 2011;6:1718–1725.
32. Akizawa H, Uehara T, Arano Y. Renal uptake and metabolism of radiopharmaceuticals derived from peptides and proteins. *Adv Drug Deliv Rev.* 2008;60: 1319–1328.